Desalination and Water Treatment
www.deswater.com

doi: 10.1080/19443994.2015.1114169

57 (2016) 22968–22979
October

Taylor & Francis
Taylor & Francis Group

Hydrodynamic design of electrochemical reactors based on computational fluid dynamics

G. Rodríguez[a], F.Z. Sierra-Espinosa[a,*], J. Teloxa[b], A. Álvarez[a], J.A. Hernández[a]

[a]*Centro de Investigación en Ingeniería y Ciencias Aplicadas, CIICAp, Universidad Autónoma del Estado de Morelos, UAEM, Av. Universidad 1001, Col. Chamilpa, Cuernavaca C.P. 62209, Morelos, Mexico, Tel. +52 777 329 7084; Fax: +52 777 329 7984; email: fse@uaem.mx (F.Z. Sierra-Espinosa)*
[b]*Departamento de Ingeniería Industrial, Universidad Politécnica de Tlaxcala, Av. Universidad Politécnica No. 1, San Pedro Xalcaltzinco, Tepeyanco, C.P. 90180 Tlaxcala, Mexico*

Received 26 March 2015; Accepted 25 October 2015

ABSTRACT

The design of electrochemical reactors using computational fluid dynamics (CFD), was investigated. A numerical methodology which considers a complete solution of transport governing equations of fluid dynamics linked together to the electrochemistry was developed. Emphasis was put on the boundary layer region, where most of the reactions between electrolyte and cathode take place, as well as mass transport, k_m. Properties of cupric sulfur ($CuSO_4 + 5H_2O$) compound were considered in the mass transport simulating as part of an electrodeposit process in a parallel plate channel filter-press cell. The proposed design method does not make use of correlations where k_m is proportional to bulk dimensionless parameters like the Reynolds (*Re*), Sherwood (*Sh*), and Schmidt (*Sc*) numbers. Electrochemical reactor´s design based on these bulk parameters requires a fully developed flow condition that warranties the accuracy of the k_m calculation. Instead, many designs of reactors can be evaluated in terms of their effective electrochemical reactions if the k_m and other variables are calculated at the electrolyte dynamic condition in the region of electroactivity, despite it is part of a fully developed flow or not. The Reynolds equations were solved using the commercial code ANSYS Fluent, and turbulence was modeled using the RNG k-ε model. The method was validated by comparing the predicted results against velocity measurements, conducted in a laboratory model of filter-press reactor using particle image velocimetry, PIV. Measured data and predictions showed a channel flow of strong velocity gradients and a recirculation zone. Calculated profiles of k_m along the reactor were compared using both the measured and predicted velocity. A comparison of reported results for the FM01-LC electrolyser against the present method demonstrates that the use of CFD allows accurate designs. This is because the electroactivity and dynamics are both taken into account in the viscous sub-layer. The method can be useful for the design of electrochemical parallel plate reactors involving mass transport and chemical reactions near the cathode operating under laminar or turbulent flow conditions.

*Corresponding author.

Presented at EuroMed 2015: Desalination for Clean Water and Energy Palermo, Italy, 10–14 May 2015. Organized by the European Desalination Society.

Keywords: Channel flow; PIV; CFD; Electrochemical reactor; Turbulence modeling

1. Introduction

The design of electrochemical reactors has been addressed by many researchers in recent years [1–3]. One of the reasons is that they are among the most promising applications like competitive production of hydrogen [4] or water treatment through the removal of contaminants [5,6] as well as the removal of low-level organics [7]. The most studied configuration is the parallel plates filter-press reactor given its simplicity of structure components and operation. This type of reactor consists of a cathode placed over the surface of one of the plates to be in contact with the electrolyte between the two parallel plates at moderate Reynolds number often in laminar regime. It has been reported that the flow dynamics of the electrolyte affects drastically the chemical reaction between the electrolyte and the electrode, leading to considering this as one difficult drawback to overpass while designing the reactor [8]. This is because velocity fluctuations typical of turbulent flows can be present even in low Reynolds number flows, such that small-scale turbulent fluctuations can be found in these flows [9]. Additionally, similarities have been observed in both low and high Reynolds flows by comparing the Reynolds stresses and small scales, using large eddy simulation (LES) and direct numerical simulation (DNS) confirming their aspects of vortex motion [9,10]. Therefore, the development of computational fluid dynamics (CFD), may impact in the design of electrochemical reactors by elucidating the dynamic condition under which the reactions take place. Indeed, a number of investigations have demonstrated the potential of CFD for investigation the effects of these hydrodynamics and performance of these reactors, as well as the effects of their geometry, dynamical behavior and performance [11–13]. Important mass transport mechanisms develop in the proximity of the electrode, inside the inner region of the boundary layer.

One popular electrolyser is the FM01-LC reactor, which is shown in Fig. 1(a) and (b). This reactor was optimized after many theoretical and experimental studies. Rivera et al. [14], analyzed the FM01-LC reactor to evaluating the design and performance under laminar and turbulent flow conditions. Also, Nelissen et al. [15] studied the reactor using a k–ω model for resolving the turbulence in a 2-D steady-state solution of the reactor electrochemistry, in a region near the wall of the cathode surface, combined with a multi-ion migration model. Distinguished elements of this reactor are the flow distributors located on inlet and outlet sections, which allow a fully developed flow in the cathode's section. The flow distributors can be observed in Fig. 1(b).

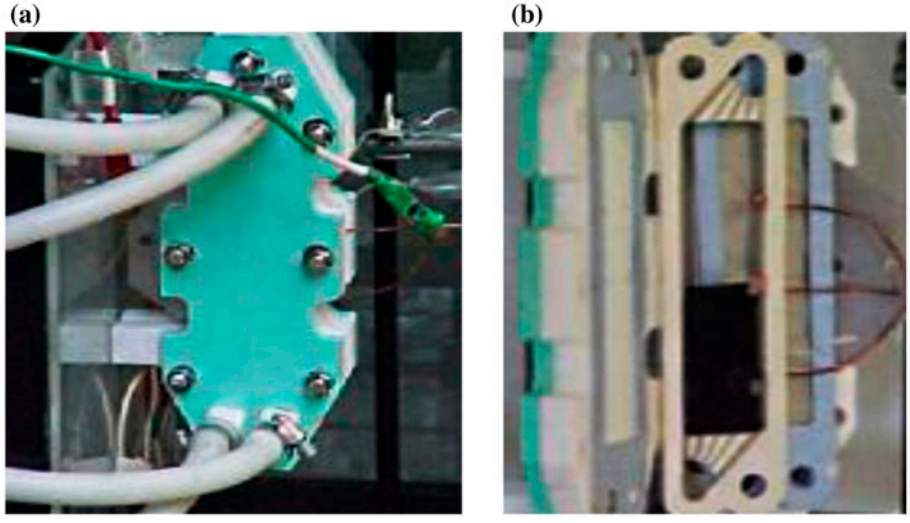

Fig. 1. Pictures of the FM01-LC filter-press parallel plates reactor installed in the laboratory: (a) front view with inlet–outlet pipes of reactor and (b) disarticulated view for ease of observing the interior channeled inlet–outlet sections as flow distributors of reactor.

The objective of the work is to solve the fluid dynamics near the electrode surface in order to calculate the mass transport, k_m, by making use of the local magnitude of velocity instead of an average outer value. This is achieved by ensuring a grid resolution that allows solving the fluid dynamics numerically at a distance to the wall small enough, within the buffer layer which is of thickness $5 \leq y^+ \leq 70$ [16], in dimensionless units. For distances inside the laminar sublayer, $0 \leq y^+ \leq 5$, the viscous effects dominate the flow behavior inducing laminar motion either in turbulent or laminar regimes. Numerical solutions at distances to the wall as near as $y^+ < 1$ were obtained using a refined grid. In this region, the differential equations for concentration and mass transport k_m were solved including the convection term, assuming no effect of the electric field. This doesn't mean that the electric current is not considered in parallel with chemical aspects. Indeed, without an electrical current the electrotransport of species is impossible. In other words, the electrodes must be polarized, which leads to stablish a flow of copper ions Cu^+ toward the cathode. Therefore, the calculations of turbulent diffusion and electroactive species concentration were conducted using the magnitude of the velocity vector near to the wall, weaving the use of the logarithmic law of the wall.

The following sections describe the fundamental equations that represent the whole system: continuity and motion equations for turbulent flow coupled with electrochemistry. Afterward, the boundary conditions applied are specified and the results are then discussed. The mass transport coefficient is calculated for a proposed configuration and compared against experimental measurements reported in the literature for the FM01-LC electrolyser. The remainder is devoted to highlighting the importance of the present CFD method for the design of electrolysers compared against the classical method that uses semi-empirical correlations based on the value of the velocity, averaged over the transversal cross-section of the reactor, which leads to inaccurate results of k_m, when the flow of electrolyte is not fully developed.

2. Methodology

2.1. Channel reactor configuration

Fig. 2(a) and (b) show the electrochemical reactor proposed in this work. The flat plate walls were made of transparent acrylic. O-ring rubber of 2 mm diameter was used to ensure a perfect sealing of water flowing throughout. The present design has the flow inlet oriented in the axial direction, while the outlet is placed to right angle, like the FM01-LC. In comparison with the FM01-LC, the present reactor is not channeled as can be seen in Fig. 2(b). For this reason the present reactor is simpler in construction.

The present design of reactor was chosen for simplicity of construction. However, the present design makes is more complex in terms of hydrodynamics, because it does not produce a fully developed flow in a short distance as the FM01-LC does [1,17–19]. A non-uniform section follows the inlet and then a rectangular zone of constant cross section is designed for the cathode location. This region of 10 cm length is equivalent to the FM01-LC design. Finally, the reactor

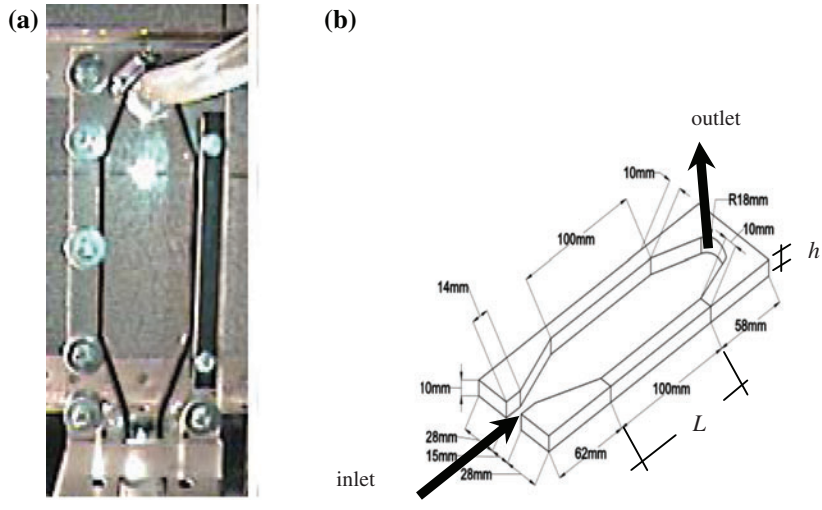

Fig. 2. Present design of filter-press parallel plates reactor: (a) front view of reactor installed in the laboratory and (b) schematic of reactor with main dimensions.

is non-uniform again until the outlet where a pipe is connected. An isometric 3-D view of the present reactor with its main dimensions is shown in Fig. 2(b).

2.2. Velocity measurements

Particle image velocimetry, PIV, is an accurate and reliable tool that has proven its capability in the study of vortex dynamics and other complex flow structures [20,21]. PIV measures the displacement of particles artificially used to seeding the flow in order to describe the flow motion. In PIV, the particles are illuminated with a sheet of laser light. One part of that light is reflected toward a CCD camera. The initial position of the particles is recorded with a first laser pulse then a second laser pulse allows for recording the final position of each particle. The time between pulses is defined according to the bulk mainstream velocity; an interval of time, $t = 21.12$ μs was used in this study. For the application of PIV, the channel was provided with a window in one lateral face of the constant cross section. This window allowed the access of light as shown in Fig. 3(a). The sheet of laser light was oriented to illuminate the reactor along the z coordinate starting at mid-height $y = h/2$. A photograph of the camera and the laser aligned with the channel constant cross section is shown in Fig. 3(b). Images of particles at frequency = 10 Hz, which is the repetition rate of the laser were obtained. Cross-correlation is used to obtain the displacement of the particles located in each interrogation area of 32 × 32 pixels [20,22].

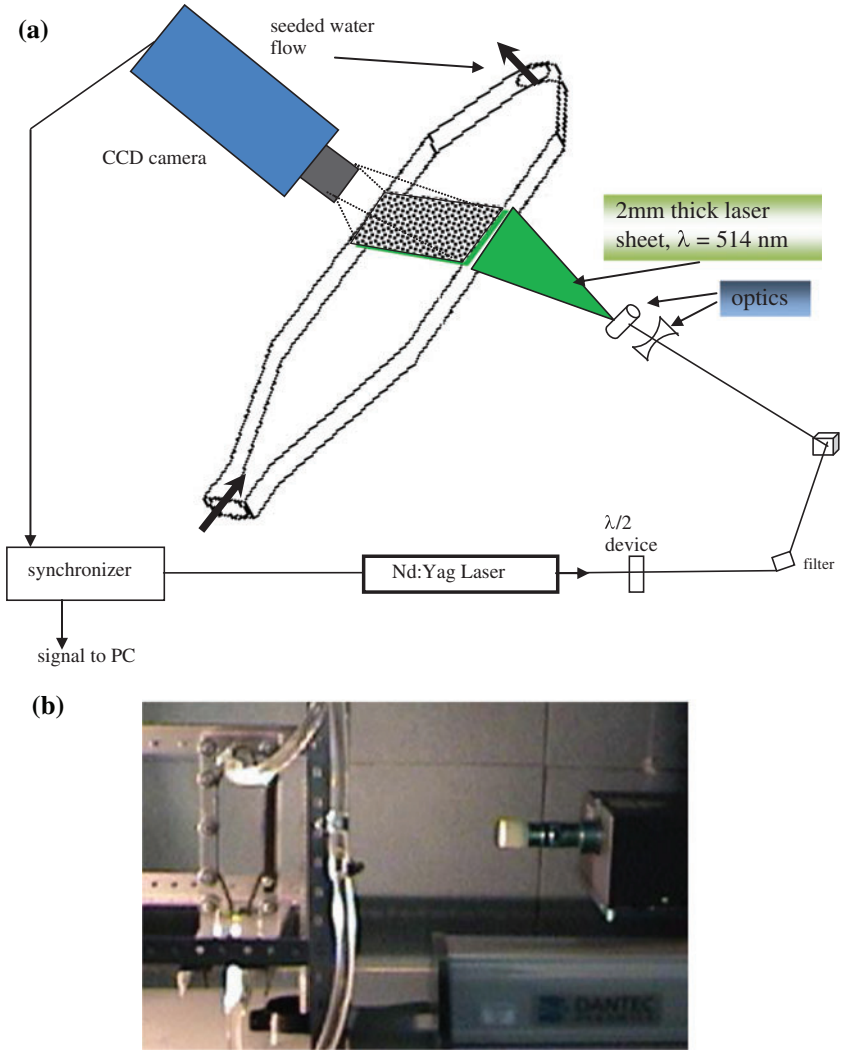

Fig. 3. Schematic of the experimental rig: (a) PIV system alignment and components and (b) Photograph of mounted PIV equipment and reactor ready for measurements.

A PIV system by Dantec Dynamics consists of a Nd:YAG double-cavity laser with light-sheet optics and a CCD camera of resolution 1280 × 1024 pixels. The camera was fitted with a Nikkor lens (focal length range of 28–60 mm) and the object distance was adjusted to obtain a field of view of 120 × 65 mm in average. The camera was synchronized with an 1100-BA processor to construct vector maps which were managed by a Flowmap software in a computer that received the signal [23]. The flow was seeded with Timirron glass particles of size ~25–50 μm. An uncertainty of mean velocities at 95% confidence was calculated to ±2% following a tested methodology [24,25].

2.3. Modeling the hydrodynamic behavior of an electrolyte

A substantial difference between chemical reactors and electrochemical reactors is the place where reactions occur. While reactions in the first ones take place over the whole volume of reactants displacement, the situation in the second ones is distinct. A theoretical description of parallel plate cell electrolysers indicates that electrochemical reactions between the electroactive species and the cathode is limited to the diffusion layer of the channel surface, say, over the cathode surface, not far from there [19]. In the present case, "far" means a very small distance, often not more than a few millimeters, or even less than that, depending on the magnitude of the *Re* number. Thus, this work focuses on the hydrodynamics in this region, which is within boundary layer thickness. The characteristics of a boundary layer developed by internal turbulent flow have been investigated since the beginning of the last century. It has two regions: one is the laminar sublayer, which is well described by the law of the wall as follows [16,26]:

$$u^+ = y^+ \tag{1}$$

where u^+ is a dimensionless velocity and y^+ a dimensionless distance to the wall. And, the second one is described by the expression know as logarithmic law of the wall:

$$u^+ = \frac{1}{k}\ln y^+ + 5.5 \tag{2}$$

where k is the constant of von Karman. The region described by Eq. (2) is connected to the laminar sub-layer by means of the buffer layer. Internal fully developed flows between infinite flat plates and cylindrical pipes have been well documented, and demonstrated by means of measurements to follow Eqs. (1) and (2). Otherwise, flows not fully developed, or flows along complex geometries present deviations when compared against such velocity profiles represented by Eqs. (1) and (2).

2.3.1. Transport equations

The transport equations used to describe a turbulent steady-state 3-D incompressible Newtonian flow were adapted from the continuity and momentum equations:

$$\frac{\partial u_j}{\partial x_j} = 0 \tag{3}$$

$$\frac{\partial}{\partial x_j}\left(u_i u_j\right) = -\frac{1}{\rho}\frac{\partial p}{\partial x_j} + \frac{1}{\rho}\frac{\partial}{\partial x_j}\tau_{ij} \tag{4}$$

which can apply to a filter-press parallel plate electrolyser; where ρ, u_{ij}, and x_i are the density, the velocity vector, and the position vector, respectively. Index denotes position, such that $i = x, y, z$. The gravity term is not considered because it does not have a direct effect in such a flow since it is balanced by the pressure gradient term [16]. The last term on the right-hand side of Eq. (4) reads for the viscous stress tensor:

$$\tau_{ij} = \mu\left(\frac{\partial u_i}{\partial x_j} + \frac{\partial u_j}{\partial x_i}\right) \tag{5}$$

where μ is dynamic viscosity. For taking into account the turbulence several methods exist. One is the Reynolds-averaged Navier–Stokes, RANS, approach, called Reynolds equations [27,28]. This method allows considering turbulence effects caused by the fluctuations of velocity u' in the direction x, and others y, z of the coordinate system, in addition to its average value, $\bar{u}$. After introducing velocity fluctuations, the equation of motion (4) becomes:

$$\frac{\partial}{\partial x_j}\left(u_i u_j\right) = -\frac{1}{\rho}\frac{\partial p}{\partial x_i} + \frac{\partial}{\partial x_j}\left[\frac{\mu}{\rho}\left(\frac{\partial u_i}{\partial x_j} + \frac{\partial u_j}{\partial x_i} - \frac{2}{3}\delta_{ij}\frac{\partial u_i}{\partial x_i}\right)\right] + \frac{\partial}{\partial x_j}\left(-\rho u_i' u_j'\right) \tag{6}$$

where bars for averaged values have been omitted. An extra term is noticed in right-hand side of Eq. (6) compared against Eq. (4). This term is called the Reynolds stress tensor, which increases the number of

variables and must be modeled in order to resolve the closure problem caused by the resulting limited number of equations [27]. One plausible approach that gives place to further development of turbulence models was the Boussinesq approximation, where an eddy viscosity μ_t is introduced [16], used in defining the k–ε model, given as follows:

$$\mu_t = \rho C_\mu k^2/\varepsilon \tag{7}$$

where C_μ is a semi-empirical non-dimensional constant of value = 0.09, k represents the turbulent kinetic energy and ε its dissipation rate, which are calculated by solving the following transport equations:

$$\rho\frac{\partial(u_i k)}{\partial x_i} = \frac{\partial}{\partial x_i}\left(\left(\mu + \frac{\mu_t}{\sigma_k}\right)\frac{\partial k}{\partial x_i}\right) + p_k - \rho\varepsilon \tag{8}$$

$$\rho\frac{\partial(u_i \varepsilon)}{\partial x_i} = \frac{\partial}{\partial x_i}\left(\left(\mu + \frac{\mu_t}{\sigma_{\varepsilon\mathrm{RNG}}}\right)\frac{\partial \varepsilon}{\partial x_i}\right) + \frac{\varepsilon}{k}(C_{1\varepsilon\mathrm{RNG}}p_k - C_{2\varepsilon\mathrm{RNG}}\rho\varepsilon) \tag{9}$$

The role of μ_t is that it represents a variable of proportionality used in the calculation of the Reynolds stress tensor as follows:

$$u_i' u_j' = -\mu_t\left(\frac{\partial u_i}{\partial x_j} + \frac{\partial u_j}{\partial x_i}\right) + \frac{2}{3}(\rho k)\delta_{ij} \tag{10}$$

which depends on the gradients of the velocity vector and the solution of the turbulence model. In this work, a turbulence model emerging from the k–ε model and the renormalization group theory is used, named RNG-k–ε model [27,29]. A detailed description of the turbulent flow viscous constant $\sigma_{k\mathrm{RNG}}$, the production of turbulence due to viscous force p_k, a constant $C_{1\varepsilon\mathrm{RNG}}$ renormalized through a function f_n for turbulent kinetic energy, and a second constant $C_{2\varepsilon\mathrm{RNG}}$ renormalized for turbulent kinetic energy is given elsewhere [28]. An expression for an effective viscosity $\mu_{\mathrm{eff}} = \mu + \mu_t$, which takes into account turbulent and molecular viscosities is provided by the RNG theory, which is cast is in terms of k and ε as follows:

$$\mu_{\mathrm{eff}} = \mu\left[1 + \sqrt{\frac{C_\mu}{\mu}}\frac{k}{\sqrt{\varepsilon}}\right]^2 \tag{11}$$

The RNG constant $C_\mu = 0.0837$. The advantage of this model compared against the k–ε is a better solution of strong velocity gradient flows by making use of filtering of scales, which allows assessing the effect of small (and fast) eddies on the large (and slow) turbulent eddies. Another benefit of this model is that it does not include any experimentally adjustable parameter [29].

Converged solutions using the *RNG-k–ε* model were obtained applying the no-slip boundary conditions at the wall. A common practice is that near the wall, in the laminar sub-layer and the buffer layer, Eqs. (3)–(10) are complemented by invoking the log-law, Eqs. (1) and (2), in order to assign a velocity value therein.

In an electrochemical flow domain, the ion motion from electrolyte, $N = \partial C_i/\partial t$, also called flux or mass transport of the electroactive species i, C, is a function of their mixed diffusion, migration, and convection, which are expressed by the right-hand side terms of the following transport equation:

$$N_{Cu^{2+}} = -\frac{\partial}{\partial x_i}(D_{Cu^{2+}} + Dt_{Cu^{2+}}) \cdot \frac{\partial}{\partial x_i}C_{Cu^{2+}} - \frac{z_i F}{RT}D_{Cu^{2+}}C_{Cu^{2+}}\frac{\partial}{\partial x_i}\phi + u_i \cdot C_{Cu^{2+}} \tag{12}$$

where sub-index Cu^{2+} accounts for the $CuSO_4 + 5H_2O$ under consideration in this work; D is the diffusion coefficient of cupric ions; Dt represents the diffusion due to turbulence effects; R is the molar gas constant; F is the Faraday constant; z is a charge of species i at temperature T; ϕ is the electric flux towards the cathode; and, finally, u is the local velocity computed from Eq. (4). The solution of Eq. (12) is simplified by depleting the migration effect. This means reducing the electric field to null. This can be done by adding an excess of supporting electrolyte to the solution. In this case, Eq. (12) reduces to:

$$N_{Cu^{2+}} = -\frac{\partial}{\partial x_i}(D_{Cu^{2+}} + Dt_{Cu^{2+}}) \cdot \frac{\partial}{\partial x_i}C_{Cu^{2+}} + u_i \cdot C_{Cu^{2+}} \tag{13}$$

Diffusion due to turbulence Dt, is resolved by invoking the analogy between heat and mass transport due to Kays–Crawford [30], which implies the following equality of turbulent Prandtl and turbulent Schmidt numbers:

$$Dt_{Cu^{2+}} = \frac{\mu_t}{\rho Sc_t} \tag{14}$$

According to this analogy, the turb'ulent Schmidt number may be defined as follows:

$$Sc_t = \left(\frac{1}{2Sc_{t\infty}} + \frac{0.3 \cdot \mu_t}{\sqrt{Sc_{t\infty}} \cdot \rho \cdot D_i} - \left(\frac{0.3 \cdot \mu_t}{\rho \cdot D_i}\right) \cdot \left(1 - \exp\left(-\frac{\rho \cdot D_i}{0.3 \cdot \mu_t \cdot \sqrt{Sc_{t\infty}}}\right)\right)\right)^{-1} \quad (15)$$

where $S_{Ct\infty}$ is a constant obtained somewhere else of value 0.85 [30].

In the case at hand, due to the divergent section of the inlet, the flow doesn't reach the fully developed status. The velocity u changes because of the vortex, which modifies the mass transport to the cathode. These changes occur in the outer edge of the boundary layer and far from the cathode's surface, but still these changes of u have an influence inside the boundary layer. This is because vigorous interactions of scales due to the production of turbulence produce increment of mass and momentum transport within the boundary layer [16].

Having solved the velocity field in the proximity of the cathode, a mass transport coefficient k_m can be formulated as follows:

$$k_{mCFD} = \frac{J_c}{Z_i \cdot F \cdot C_i} \quad (16)$$

where J_c represents a density of current to the surface of the cathode in A m^{-2}; Z_i is the electron interchange between the electroactive species and the cathode (in this case equal to 2); F is the constant of Faraday, $F = 96{,}485$ A s mol^{-1}; and C_i represents the concentration of electroactive species (in this case $C_i = 10$ mol m^{-3}). Eq. (16) can be reduced if the density of current is expressed in terms of the mass transport N_i, see Eq. (13), as follows:

$$J_c = Z_i \cdot F \cdot N_i \quad (17)$$

Therefore, the mass transport coefficient reads:

$$k_{mCFD} = \frac{N_i}{C_i} \quad (18)$$

A non-dimensional concentration of electroactive species i, in the logarithmic layer, is calculated using Eq. (2) assuming a Launder–Spalding distribution, in substitution of concentration C_i in Eq. (18) [30]:

$$C^+ = Sc_t \cdot \left(\frac{1}{\kappa} \cdot \ln \cdot y^+ + 5.5 + P_c\right) \quad (19)$$

When sufficient grid refinement this changes to:

$$C^+ = Sc_t \cdot \left(\frac{u}{U^*} + P_c\right) \quad (20)$$

For the viscous sub-layer, concentration C^+ is obtained by:

$$C^+ = Sc \cdot y^+ \quad (21)$$

In Eq. (19), P_c is a term that takes into account the displacement between the Nernst diffusion layer and the pure dynamics boundary layer, given by:

$$P_c = A \cdot \left[\left(\frac{Sc}{Sc_t}\right)^{\frac{3}{4}} - 1\right] \quad (22)$$

In summary, the present investigation considers cupric sulfur ($CuSO_4 + 5H_2O$) compound as a part of the water flow to produce electrodeposition of copper, Cu, on the cathode, in a parallel plate channel filter-press cell. The following electrochemical reaction is taking place on the basis of the reactor, which defined the cathode´s location:

$$Cu^{2+} + 2e^- \rightarrow Cu \quad (23)$$

Eq. (23) expresses the formation of Cu molecules taken from the electrolyte as a consequence of applying an electrical current on the cathode's surface. When oxygen is still present in the flow there must be another reaction competing for the available electric current with the first one (Eq. (23)) as follows:

$$O_2 + 4H^+ + 4e^- \rightarrow 2H_2O \quad (24)$$

2.3.2. Empirical correlation equations

A typical procedure for designing an electrochemical reactor must ensure that the hydrodynamic behavior of the flow in the parallel plate channel belongs to fully developed flow. Under this condition, k_m can be calculated using correlations of the kind:

$$k_m = a\bar{v}^b \quad (25)$$

where $\bar{v}$ is the average flow velocity at the transversal cross-section of a rectangular channel, while the magnitude of a and b are obtained experimentally. Furthermore, the following expressions are employed:

$$k_m = D\left(\frac{Sh}{d_e}\right) \tag{26}$$

$$Sh = aRe^b Sc^c Le^e \tag{27}$$

where *Sh*, *Re*, *Sc*, and *Le* are the Sherwood number, Reynolds number, Schmidt number, and the dimensionless length group number, respectively, and *a*, *b*, *c*, and *e* are empirical constants [1,31]. Empirical constants and averaged magnitude of the velocity over the transversal cross-section of the electrolyser limits the validity of Eq. (21) to fully developed flows. Therefore, this procedure can't be applied to configurations like the reactor proposed in this work since they meet the condition of fully developed flow.

The computation of k_m using the finite volume approach, Eqs. (3)–(17), constitutes an alternative method for the design of electrolysers, which is not restricted to the fully developed flow condition in the channel. The numerical solution of the velocity field allows the local determination of the mass transport from the electrolyte toward the cathode, avoiding the use of gross average magnitudes. In the next sections, the alternative method is applied to the proposed parallel plate reactor and to the FM01-LC, and the results are compared.

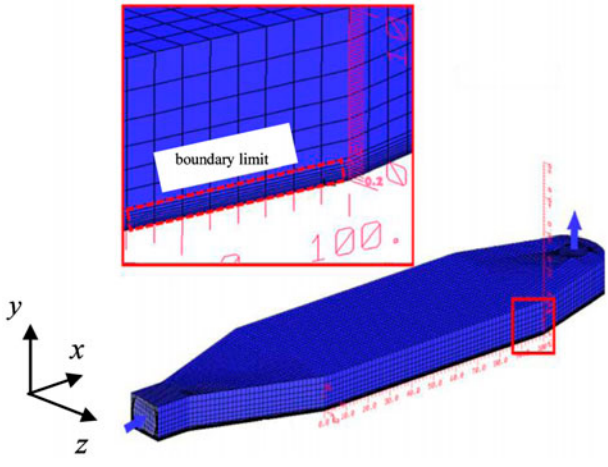

Fig. 4. Computational grid used for the CFD simulations of flow in the reactor.

2.3.3. Computational grid

All solutions for the fluid flow in the reactor were obtained in steady state using a program Fluent [28]. The boundary conditions used were a mass flow rate of inlet = 0.025 kg s^{-1}; all velocity component vanish at all the rigid walls; and outflow at the exit. The solutions were obtained using a SIMPLE algorithm for coupling the velocity to pressure terms in the Reynolds equations. Turbulence was addressed employing a model based on the renormalization group theory, RNG [29,32,33]. A computational grid of 1.8×10^5 elements distributed with higher density of elements in the boundary layer, was used, which is shown in Fig. 4. A grid refinement was conducted in order to demonstrate independence of results. Table 1 shows the data of each grid tested and the grid convergence index, GCI [34], which was calculated using the velocity results for ($x = 3L/4$, $y = h/2$) position in the reactor. Independence is better as the factor GCI approximates unity. For the present work Grid 4 was judged appropriate. A test of four grids was conducted for the whole profile of velocity on the same position (x, y), which is shown in Fig. 5. As observed, as the number of elements grows the velocity converges.

3. Results

3.1. Validation of numerical model

Experimental data from PIV measurements of velocity were used to test the accuracy of numerical method. A comparison of results was conducted using profiles of the velocity component u in the x direction. Profiles were oriented perpendicularly to the main direction of the flow for the planes $y = h/10$, $y = h/2$, for a position $x = L/2$. The results are shown in Fig. 6.

As observed in this figure, the numerical predictions reproduce the experimental data with good

Table 1
Grid independence test data

Grid number	Number of elements	u velocity (m s^{-1})	Maximum volume of cell (mm^3)	Size ratio (R)	Grid velocity relation (ε)	GCI (%)
1	87,300	0.056	2.49	–	–	–
2	287,400	0.051	1.67	1.5	0.09	55.4
3	593,300	0.053	1.32	2	0.02	7.4
4	1,782,700	0.053	0.922	2.5	0.01	2.4

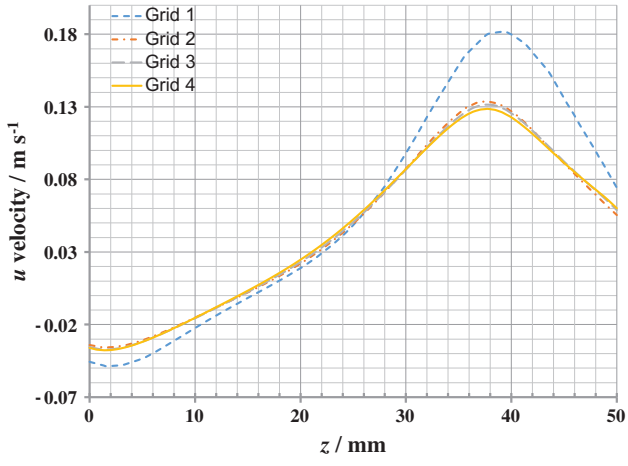

Fig. 5. Grid independence test in whole width of reactor for position $3L/4$.

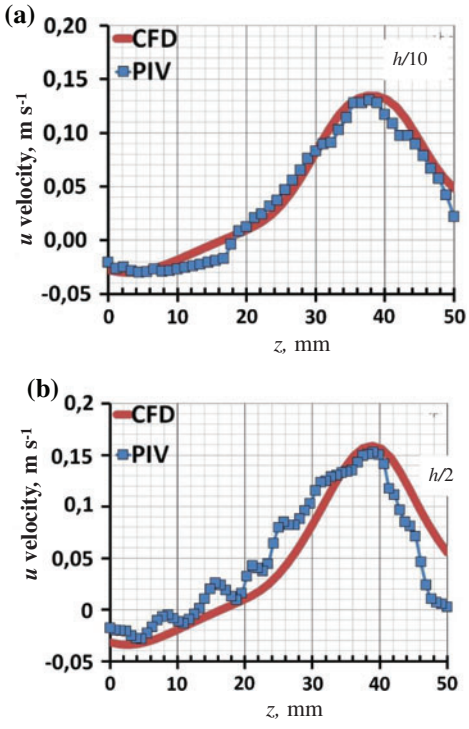

Fig. 6. Comparison of CFD results against experimental data from measurements using PIV velocimetry in the plane at mid-length of reactor, $L/2$: (a) velocity profile on distance to the wall $y = 0.001$ m and (b) velocity profile on distance to the wall $y = 0.005$ m.

agreement, with less than 10% error. The best approximation is for plane $h/10$, distance to the wall $y = 0.001$ m (Fig. 6(a)) compared against plane $h/2$, $y = 0.005$ m (Fig. 6(b)). This is because the flow is laminar in the proximity of the wall. As distance to the wall increases the gradients of velocity in all directions represent an obstacle for any prediction of turbulent flow. Despite this the discrepancies between predictions and measurements in the plane $h/2$ are still acceptable.

Focusing on the right-hand side wall of the reactor, the velocity profiles show negative values of u until a distance of 0.018 m in direction of z. Afterward the velocity increases until a maximum of $u = 0.014$ m s^{-1} and then falls to 0 on the other extreme of the reactor.

The results of Fig. 6 indicate that the flow in the reactor has two main regions: a region of positive velocity in the direction of x over the right-hand side; and a region of negative velocity possibly indicating recirculation of flow on the left-hand side of the reactor. Both, predictions and data reveal that the flow in the reactor is not fully developed. The flow described by the profiles of velocity in Fig. 6 is described by stream lines in Fig. 7. The stream lines confirm a big recirculating flow cell on the left-hand side of the reactor. This flow represents a challenge from the point of view of reactor´s efficiency. A design based on the correlations method defined by Eqs. (25)–(27) is inappropriate because it was conceived for a fully developed flow. Therefore, a recirculating flow like this is out of question for such a method.

However, since the electrochemical reactions occur in the diffusion layer as already discussed, their computation based on the numerical method described by Eqs. (3)–(19) is appropriate because it takes into account the influence of a recirculation flow, even with negative velocity like the one observed in the region $0 \leq z \leq 0.018$ m.

3.2. Electrochemical predictions

The results are focused on the magnitude of the mass transport k_m. A direct comparison of results is

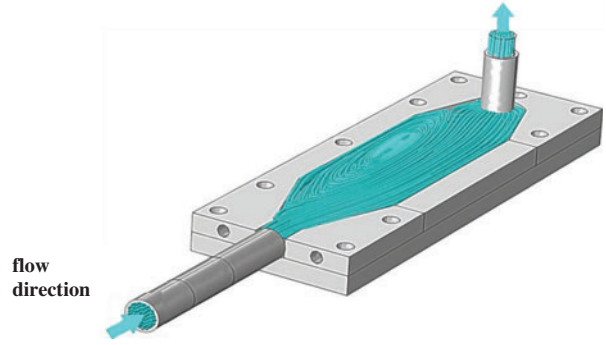

Fig. 7. CFD prediction of recirculating flow path in the form of stream lines, for flow rate = 0.025 kg s^{-1}.

made against the FM01-LC electrolyser, both working on the same condition: a mass flow rate of 0.025 kg s^{-1}. The results correspond to three positions along the reactor section L, plane $h/2$, shown in Fig. 8.

The results of k_m profiles can be observed in Fig. 9(a–c). Continuous lines are used to indicate the predicted k_m from Eq. (15), and PIV measured data of velocity; dotted lines describe the results for the FM01-LC reactor. The results were plotted in logarithmic scale to visualizing the trend of k_m, as well as ease of comparison among FM01-LC and present reactor designs.

The k_m results in Fig. 9(a–c) reflect the velocity variations for each reactor design. The flow condition is changing along L. In the case of the present reactor, the velocity varies from small values to maximum due to the recirculation of flow. Although some are negative velocity, the computation of k_m is made considering the absolute value. A small velocity may impact on the calculation of k_m. However, as observed the effect is very little in terms of k_m slope, which reflects a small difference compared against the FM01-LC reactor results, where the flow develops with little variation, due to the affectivity of its channeled

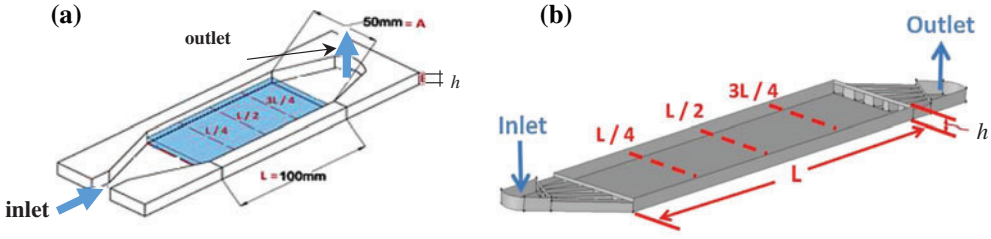

Fig. 8. Location of profiles for comparison of results: (a) Present design with inlet/outlet sections indication. Marked rectangular section in the inferior plate of the reactor was designed for cathode location and (b) design of FM01-LC cell.

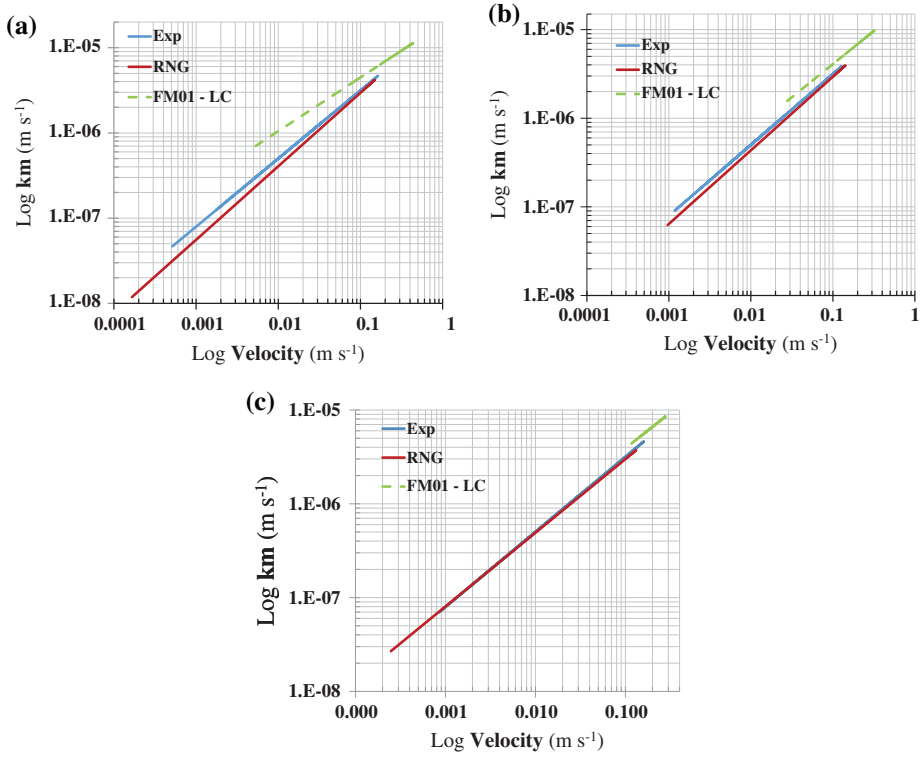

Fig. 9. Mass transport coefficient k_m of present design compared against the commercial FM01-LC cell: (a) Position $L/4$, (b) Position $L/2$ and (c) position $3L/4$. See Fig. 6.

section. As expected, k_m varies according to the local value of velocity. This is why the magnitude of k_m covers more decades for the present design, and only few decades for the FM01-LC reactor. This effect augments with position along L, such that for $x = 3L/4$ the results, Fig. 9(c), shows a very good agreement between present and FM01-LC designs.

In summary, the results of Fig. 9(a–c) indicate that k_m decreases, not vanishes, for regions where the flow reverses, and it grows for regions where the flow gets higher velocity, comparable to the FM01-LC reactor. In Fig. 9(a) for $L/4$, k_m presents maximum differences of slope and magnitude among both reactors; whereas minimum differences correspond to position $x = 3L/4$.

Vázquez et al. [11] reported results of $k_m = 1.1 \times 10^{-5}$ m s^{-1} for a channel configuration provided with manifold distribution of flow, similar to the FM01-LC reactor, for inlet flow condition of 0.065 m s^{-1} (roughly equivalent to present 0.025 kg m s^{-1}) which was calculated using the correlations expressed through Eqs. (19)–(21). These results were compared against other data from the literature with good agreement [35]. Based on the results of Fig. 9(a–c), the calculated k_m values range from 3×10^{-8} to 0.7×10^{-5} m s^{-1}, which is close to their range of k_m. It is worth to remind that present results were obtained in a reactor with no manifold flow distribution, which is low cost compared to manifold construction. These figures show that the method proposed here based on the use of CFD calculations may represent an attractive option for evaluating any design of electrochemical reactor. This means, no matter if complex flow distribution paths are found in the cathode section of the reactor, which is far from fully developed flow. A reactor performance evaluation reveals the suitability of any design compared against typical designs.

The simplicity of the geometry configuration of the reactor proposed here represents a major advantage in terms of ease of construction and costs compared against channeled configurations like the one used in the FM01-LC.

4. Conclusions

A simple parallel plate electrochemical reactor was studied experimentally and numerically in order to verify a numerical method based on the boundary layer, proposed as a tool in the process of electrochemical reactor's design. The velocity of an electrolyte proper for electrochemical applications with a Reynolds number, Re_i = 2,200, based on the average inlet velocity, and the diameter at the inlet section of the reactor, was measured experimentally using PIV, and resolved with the program Fluent. The solution obtained with the RNG model for turbulence showed good agreement with the experimental data of velocity. Thus, this method was used to analyze the mass transport coefficient k_m and compare the results against the FM01-LC electrolyser, which use manifolds to stabilize the flow. Results of k_m in a range between 3×10^{-8} and 0.7×10^{-5} m s^{-1} were obtained for the proposed reactor without any manifold flow distribution. This is in range with experimental data reported for the FM01-LC electrolyser. These results show that the method based on CFD represent an attractive option for evaluating any electrochemical reactor configuration, even with complex flow distributions far from fully developed flow. The simplicity of the geometry configuration of the reactor proposed here represents a major advantage in terms of ease of construction and costs, compared against channeled inlet section configurations like the one used in the FM01-LC.

Acknowledgments

Authors thank the funds from the National Council for Science and Technology Conacyt, under grant number: CB2008-102167. G. Rodríguez thanks the financial support from postgraduate program-Conacyt during the PhD period.

Nomenclature

d_e	—	equivalent hydraulic diameter of the rectangular flow channel (m)
$h/2$	—	mid-height plane in the channel local mass transport coefficient (m s^{-1})
k_m	—	local mass transport coefficient (m s^{-1})
$k_m$exp	—	experimental local mass transport coefficient (m s^{-1})
$k_m$num	—	numerical local mass transport coefficient (m s^{-1})
L	—	length of the channel in the constant cross-section
p	—	pressure (Pa)
Sc	—	Schmidt number
Sh	—	Sherwood number
Re	—	Reynolds number: $Re = \frac{d u_{inlet}}{\nu}$
u_{ij}	—	vector (m s^{-1})
u	—	velocity in the main direction of flow (m s^{-1})
u_{inlet}	—	velocity at the inlet of the channel (m s^{-1})
u^+	—	non-dimensional velocity, $u^+ = \frac{u}{U^*}$
U^*	—	friction velocity, $U^* = \sqrt{\frac{\tau_w}{\rho}}$
x, y, z	—	Cartesian coordinates (m)
x_i	—	position vector (m)
y^+	—	non-dimensional distance to the wall, $y^+ = \frac{\rho U^* y}{\mu}$

X — channel width (m)
ε — turbulent dissipation rate
μ — dynamic viscosity (kg m^{-1} s^{-1})
v — kinematic viscosity (Pa s)
ρ — density (kg/m^3)
λ — wave length (514 nm)
τ_w — shear stress at the wall, $\tau_w = \mu \frac{du}{dy}$

References

[1] F.C. Walsh, A First Course in Electrochemical Engineering, The Electrochemical Consultancy, Romsey, UK, 1993.
[2] C. Ponce de León, G.W. Reade, I. Whyte, S.E. Male, F.C. Walsh, Characterization of the reaction environment in a filter-press redox flow reactor, Electrochim. Acta 52 (2007) 5815–5823.
[3] A. Frías-Ferrer, L. González-García, V. Saéz, C. Ponce de León, F.C. Walsh, The effects of manifold flow on mass transport in electrochemical filter-press reactors, AIChE J. 54(81) (2008) 1–823.
[4] U.M. López-García, P.E. Hidalgo, J.C. Olvera, F. Castañeda, H. Ruiz, G. Orozco, The hydrodynamic behavior of a parallel plate electrochemical reactor, Fuel 110 (2013) 162–170.
[5] C. Ponce de Leon, D. Pletcher, Removal of formaldehyde from aqueous solutions via oxygen reduction using a reticulated vitreous carbon cathode cell, J. Appl. Electrochem. 25 (1995) 307–314.
[6] M.R.V. Lanza, R. Bertazzoli, Cyanide oxidation from wastewater in a flow electrochemical reactor, Ind. Eng. Chem. Res. 41 (2002) 22–26.
[7] A. Alvarez-Gallegos, D. Pletcher, The removal of low level organics via hydrogen peroxide formed in a reticulated vitreous carbon cathode cell, Part 1. The electrosynthesis of hydrogen peroxide in aqueous acidic solutions, Electrochim. Acta 44 (1998) 853–861.
[8] A.N. Colli, R. Toelzer, M.E.H. Bergmann, J.M. Bisang, Mass-transfer studies in an electrochemical reactor with a small interelectrode gap, Electrochim. Acta 100 (2013) 78–84.
[9] A.H. Herbst, P. Schlatter, D.S. Henningson, Simulations of turbulent flow in a plane asymmetric diffuser, Flow Turbul. Combust. 79 (2007) 275–306.
[10] I. Recktenwald, N. Alkishriwi, W. Schröder, PIV–LES analysis of channel flow rotating about the streamwise axis, Eur. J. Mech. B. Fluids 28 (2009) 677–688.
[11] L. Vázquez, A. Alvarez-Gallegos, F.Z. Sierra, C. Ponce de León, F.C. Walsh, Prediction of mass transport profiles in a laboratory filter-press electrolyser by computational fluid dynamics modelling, Electrochim. Acta 55(10) (2010) 3446–3453.
[12] L. Vázquez, A. Alvarez-Gallegos, F.Z. Sierra, C. Ponce de León, F.C. Walsh, Simulation of velocity profiles in a laboratory electrolyser using computational fluid dynamics, Electrochim. Acta 55(10) (2010) 3437–3445.
[13] L. Vázquez, A. Alvarez-Gallegos, F.Z. Sierra, C. Ponce de León, F.C. Walsh, CFD evaluation of internal manifold effects on mass transport distribution in a laboratory filter press flow cell, J. Appl. Electrochem. 43 (2013) 453–465.
[14] F.F. Rivera, C. Ponce de León, F.C. Walsh, J.L. Nava, The reaction environment in a filter-press laboratory reactor: The FM01-LC flow cell, Electrochim. Acta 161 (2015) 436–452.
[15] G. Nelissen, B. Van Den Bossche, J. Deconinck, A. Van Theemsche, C.D. Adrian, Laminar and turbulent mass transfer simulations in parallel plate reactor, J. Appl. Electrochem. 33 (2003) 863–873.
[16] H. Schlichting, K. Gersten, Boundary Layer Theory, eighth ed., Springer-Verlag, Berlin-Heidelberg, 2000.
[17] E.P. Rivero, F.F. Rivera, M.R. Cruz-Díaz, E. Mayen, I. González, Numerical simulation of mass transport in a filter press type electrochemical reactor FM01-LC: Comparison of predicted and experimental mass transfer coefficient, Chem. Eng. Res. Des. 90 (2012) 1969–1978.
[18] F.C. Walsh, G. Mills, Electrochemical techniques for a cleaner environment, Chem. Ind. 15 (1993) 576–580.
[19] F.C. Walsh, G. Reade, Design and performance of electrochemical reactors for efficient synthesis environmental treatment. Part 1. Electrode geometry and figures of merit, Analyst 119 (1994) 791–796.
[20] R.D. Keane, R.J. Adrian, Theory of cross-correlation analysis of PIV Images, J. Appl. Sci. Res. 49 (1992) 1–27.
[21] B. Ganapathisubramani, E.K. Longmire, I. Marusic, S. Pothos, Dual-plane PIV technique to determine the complete velocity gradient tensor in a turbulent boundary layer, Exp. Fluids 39(2) (2005) 222–231.
[22] J. Westerweel, On velocity gradients in PIV interrogation, Exp. Fluids 44(5) (2008) 831–842.
[23] Dantec Dynamics, Flow Manager User's guide, Tonsbakken, Skovlunde Denmak, 2009.
[24] J.H.W. Coleman, W.G. Steele, Experimentation and Uncertainty Analysis for Engineers, John Wiley, New York, NY, 1989.
[25] D.J. Forliti, P.J. Strykowski, K. Debatin, Bias and precision errors of digital particle image velocimetry, Exp. Fluids 28(5) (2000) 436–447.
[26] J.O. Hinze, Turbulence, Mc Graw Hill, New York, NY, 1975.
[27] W.D. McComb, The Physics of Fluid Turbulence, Oxford Univ. Press, New York, NY, 1994.
[28] ANSYS Fluent, User's Guide, ANSYS, Inc., Southpointe, 2600 ANSYS Drive, Canonsburg, PA, USA, 2011.
[29] V. Yakhot, S.A. Orszag, Renormalization group analysis of turbulence. I. Basic theory. J. Sci. Comput. 1(1) (1986) 3–51.
[30] B.E. Launder, D.B. Spalding, The numerical computation of turbulent flows, Comput. Methods Appl. Mech. Eng. 3 (1974) 269–289.
[31] F. Goodridge, K. Scott, Electrochemical Process Engineering, Plenum Pres, New York, NY, 1995.
[32] U. Frisch, Turbulence, Cambridge University Press, Cambridge, 1995.
[33] J. Ferziger, M. Perić, Computational Methods for Fluid Dynamics, Springer, Germany, 1996.
[34] P.J. Roache, Fundamentals of Computational Fluid Dynamics, Hermosa, New Mexico, 1998.
[35] C.J. Brown, D. Pletcher, F.C. Walsh, J.K. Hammond, D. Robinson, Local mass transport effects in the FM01 laboratory electrolyser, J. Appl. Electrochem. 22 (1992) 613–619.